

*Full Length Research Paper*

# Heat and fluid flow analysis in gas turbine blade cooling passages with semicircular turbulators

M Alhajeri\* and H. Alhamad Alhajeri

Mechanical P and R Engineering Department, Faculty of Technological Studies, PAAET, Kuwait.

Accepted 29 October, 2009

**This paper reports a numerical investigation of heat transfer and flow characteristics in a two-dimensional u-tube over semicircular turbulators. Repeated semicircular turbulators (ribs) are used inside a cooling passage to promote turbulence and enhance convective heat transfer in gas turbine blades to create higher thrust-to-weight ratios. The u-tube has a 180° bend while the turbulators are distributed on both walls in a staggered arrangement where the ratio  $h/d$  is 0.1 and the spacing ratio  $S/d$  is 1. Four Reynolds numbers, 40,000, 60,000, 80,000 and 95,000 are considered. The predicted velocity and heat transfer in the u-tube concur with measurement data from the relevant literature. High velocity regions occur near the lower wall in the downstream duct while the heat transfer is increased in the downstream duct. Furthermore, the greater the Reynolds number beyond a certain value (moderate Reynolds numbers), the smaller the increment in Nusselt number.**

**Key words:** Blade cooling, CFD, turbulators, gas turbine

## INTRODUCTION

Gas turbine blades have to be heavily cooled due to extremely high turbine inlet temperatures. The allowable metal temperature is much lower than the combustion chamber hot gas temperature; as such, the blade material temperature has to be lowered using a combination of cooling methods. In order to increase the internal heat transfer, turbulence promoters such as ribs are generally used, distributed in both walls of the channel in a staggered arrangement in order to disrupt the boundary layer periodically, resulting in high turbulence levels and effectively mixing the coolant core flow.

Both Metzger and Sahn's (1986) heat transfer experiment, Park and Lau's (1998) heat and mass transfer experiment in smooth 180° bends showed steep increases in heat transfer, reaching the maximum value at the exit of the bend leading into the second pass. Schabacker and Bölcs's (1998) PIV study of a 180° bend region with smooth walls identified several large-scale flow structures in the duct, including recirculation zones in the upstream and downstream corners and a large separation bubble hugging the inside wall downstream of the divider tip. Meanwhile, Besserman and Tanrikut (1992) calculated the flow characteristics of a 180° bend using a  $k-\epsilon$  model,

demonstrating that an advanced treatment of the boundary conditions was essential when the  $k-\epsilon$  model was used. A computational study on a two-pass duct with 90° ribs by Zhao and Tao (1997) used a  $k-\epsilon$  model with wall functions to simulate the flowfield, obtaining reasonably good agreement between numerical and experimental results. Furthermore, Taslim (2000); Ligrani et al. (2003) and Han et al. (2001) provided good reviews of methods used for internally cooling the rectangular channel.

Sewall and Tafti (2006) conducted a large eddy simulation of the 180° bend in a stationary ribbed duct. The studied domain included three ribs upstream of the bend region and three ribs downstream of the bend, with an outflow extension added to the end. The results indicated that heat transfer increased with the presence of a rib. Including a rib in the bend increased the friction factor in the bend by 80% and increased the heat transfer augmentation by approximately 20%. Amro et al. (2007) experimentally studied heat transfer in a ribbed cooling channel and found that the most promising rib arrangement for leading edge cooling is a rib with 45° angle and double-sided fully overlapped ribs in the arc area. These ribs provide uniform heat transfer in the arc area as well as a high number of heat transfer coefficients in the channel.

Aroon et al. (2006) presented numerical predictions of a hydrodynamic and thermally developed turbulent flow

\*Corresponding author. E-mail: [eaxalm@yahoo.com](mailto:eaxalm@yahoo.com)

for a rotating duct with square ribs aligned in a normal manner to the main flow direction. Tafti (2005) conducted additional computational simulations in a ribbed square duct with a rib height-to-hydraulic diameter ratio of 0.1 and rib pitch-to-rib height ratio of 10. Furthermore, Jia et al. (2005) performed a numerical analysis of heat transfer enhancement in square ducts with V-shaped ribs. They found that, both downstream and upstream of the turn, the V-shaped ribs resulted in better heat transfer enhancement than transverse straight ribs in ducts.

Most previous work on the internal cooling of gas turbines focused on square tabulator ribs. The current paper conducts a computational fluid dynamics (CFD) investigation of flow and heat transfer in a rectangular duct with round tabulator ribs mounted in a staggered arrangement.

**MATHEMATICAL MODEL**

The RNG  $k-\epsilon$  turbulence model and a well-established standard wall function were chosen for the near wall treatment. The equations governing the steady flow of two-dimensional, incompressible turbulent flow include differential expressions for mass and momentum, as given by:

$$\frac{\partial}{\partial x_i}(\rho u_i) = 0 \tag{1}$$

$$\frac{\partial}{\partial x_j}(\rho u_i u_j) = -\frac{\partial p}{\partial x_i} + \frac{\partial}{\partial x_j}(\rho v_t \frac{\partial}{\partial x_i} u_i) - \frac{\partial}{\partial x_j}(\overline{\rho u_i^o u_j^o}) \tag{2}$$

Where;  $\rho$ ,  $u$ ,  $u'$ ,  $P$ , and  $v_t$  are bulk density, mean velocity, fluctuating velocity, mean pressure, and laminar viscosity, respectively. The stress tensor  $\overline{u_i^o u_j^o}$  is given as:

$$\overline{u_i^o u_j^o} = -v_t \left( \frac{\partial u_i}{\partial x_j} + \frac{\partial u_j}{\partial x_i} \right) + \frac{2}{3} k \delta_{ij} \tag{3}$$

Where;  $v_t$  is turbulent or eddy viscosity,  $k$  is the kinetic energy of turbulence, and  $\delta_{ij}$  is the Kronecker delta ( $\delta_{ij} = 1$  for  $i = j$  and  $\delta_{ij} = 0$  for  $i \neq j$ ).

The RNG  $k-\epsilon$  model was developed in 1986. The model used here is based on the work done by Orszag et al. (1993) In the RNG formulation, the turbulent viscosity,  $v_t$ , is evaluated by  $(v_{eff} - v_l)$ , where  $v_l$  is the laminar viscosity. The effective viscosity,  $v_{eff}$ , is computed by:

$$v_{eff} = v_l \left( 1 + \sqrt{\frac{C_\mu}{v_l} \frac{k}{\epsilon}} \right)^2 \tag{4}$$

Where;  $C_\mu=0.0845$ . The kinetic energy of the turbulence,  $k$ , and its dissipation rate,  $\epsilon$ , is governed by separate transport equations. The  $k$  and  $\epsilon$  transport equations are:

$$\frac{\partial}{\partial x_i}(\rho U_i k) = \frac{\partial}{\partial x_i}(\alpha \rho v_t \frac{\partial k}{\partial x_i}) + P_k + \rho \epsilon \tag{5}$$

$$\frac{\partial}{\partial x_i}(\rho_g U_i \epsilon) = \frac{\partial}{\partial x_i}(\alpha \rho v_t \frac{\partial \epsilon}{\partial x_i}) + \frac{\epsilon}{k}(C_{\epsilon 1} P_k - C_{\epsilon 2} \rho \epsilon) - \rho R \tag{6}$$

Where;  $\alpha$  is an inverse Prandtl number that may be obtained from the following equation (Orszag et al. [14]):

$$\left| \frac{\alpha - 1.3929}{\alpha_0 - 1.3929} \right|^{0.6321} \left| \frac{\alpha + 2.3929}{\alpha_0 + 2.3929} \right|^{0.3679} = \frac{v_l}{v_{eff}} \tag{7}$$

Where;  $\alpha_0 = 1$ . The turbulence production,  $P_k$ , is evaluated by:

$$P_k = \rho^2 v_t \left( \frac{\partial U_i}{\partial x_j} + \frac{\partial U_j}{\partial x_i} \right) \left( \frac{\partial U_i}{\partial x_j} \right) \tag{8}$$

The rate of strain term,  $R$ , in the  $\epsilon$  equation is expressed as:

$$R = \frac{C_\mu \eta^3 (1 - \eta / \eta_0) \epsilon^2}{1 + \beta \eta^3} \frac{1}{k} \tag{9}$$

$$\eta = \frac{k}{\epsilon} (2S_{ij}^2)^{1/2} \tag{10}$$

$$S_{ij} = \frac{1}{2} \left( \frac{\partial U_i}{\partial x_j} + \frac{\partial U_j}{\partial x_i} \right) \tag{11}$$

Where;  $\beta = 0.015$  and  $\eta_0 = 4.38$ . According to RNG theory, the constants in the turbulent transport equations take the values of  $C_{1\epsilon}=1.42$  and  $C_{2\epsilon}=1.68$ , respectively.

**Geometry, grid, and boundary conditions**

The tabulator or rib is modeled as a half-circular cylinder (semicircular). The center of the circle is at the wall of the duct. The radius of the circle is 1. The u-tube has four walls: two upstream of the bend and two downstream. Each wall is simulated with four ribs. The ratio of the spacing between the ribs to the diameter of the duct,  $S/d$ , is 1, as shown in Figure 1. The u-tube has a width of  $d$

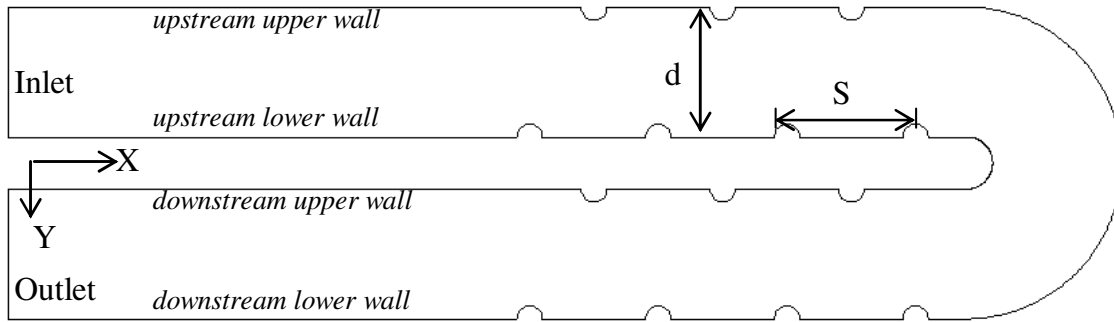


**Figure 1.** Schematic of rib-roughened u-duct and computational domain.

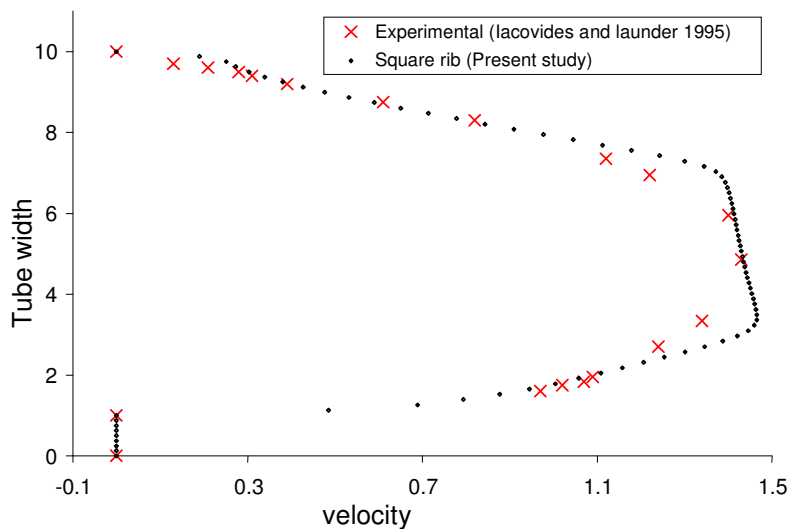


**Figure 2.** Comparison with experimental results obtained by Iacovides and Launder [15] for velocity profile at  $x = 36$  upstream of the bend for square rib

and a sharp  $180^\circ$  bend with a mean radius,  $r_b/d$ , equal to 0.65. The ribs are distributed on both walls in a staggered arrangement. The ratio of the radius of the rib to the diameter of the tube,  $r/d$ , is 0.1. The ribs closest to the bend are  $0.45d$  from the entrance and exit of the bend.

The mesh is uniform throughout the geometry, having a total size of 58,000 quadrilateral cells. The mesh is a structured-type cell (Quad cell) generated in Gambit. The CFD code used in this study is Fluent. The domain is a two-dimensional plane and has three boundaries, as shown in Figure 1.

The boundary conditions at the wall set as wall cell use the standard wall function. A no-slip velocity boundary condition was applied at the wall; in other words, both the  $x$  and  $y$  components of velocity are constrained to zero. The inflow boundary or the main inlet is set as a constant  $x$  component and zero  $y$  component of the velocity. Based in the inlet conditions and the width of the tube, the Reynolds numbers ( $Re$ ) here is 95,000. At the outflow

boundary, the velocities are left free, resulting in the default boundary condition of zero stress in normal and tangential directions.

### Validation and grid independency

Most studies in the field of internal turbine cooling using tabulators or ribs have used square ribs; no studies using semicircular ribs were found to provide results for comparison with the results of the present study. Therefore, studies using the same geometry and boundary conditions but with square ribs are compared with obtainable results from literature. Iacovides and Launder (2006) conducted an excellent experimental study using similar geometry and boundary conditions at a high Reynolds number (that is, 95,000). Figure 2 shows the comparisons with Iacovides and Launder's (1995) experimental results for a velocity profile at  $x = 36$  upstream of the bend

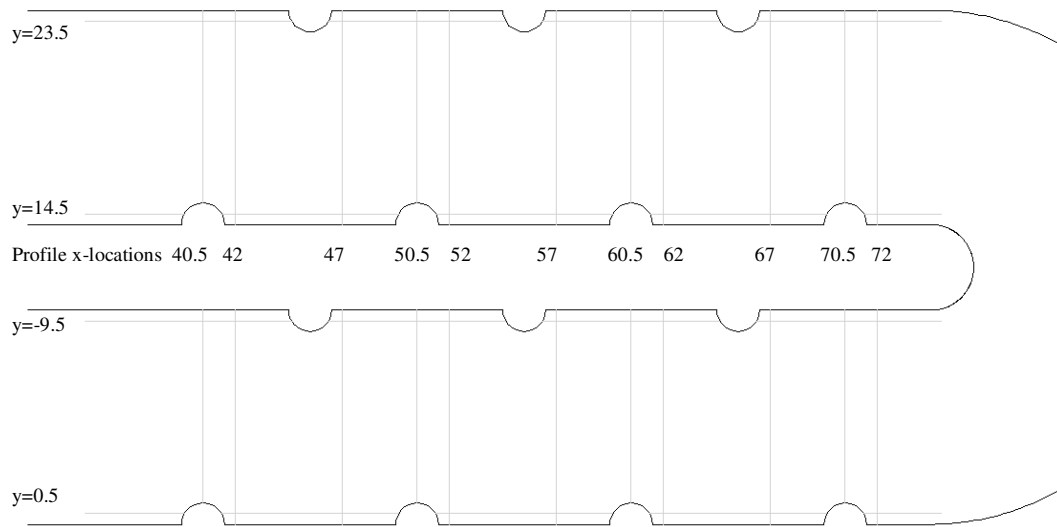


**Figure 3.** Locations of the velocity profiles in  $x$  and  $y$  axes.

for a square rib. The two profiles are closely matched, especially in the area close to the wall, the area of interest in the current study. In the middle of the duct, the experimental results rather than the computational results show more developed flow.

Prior to conducting any comparisons with other studies, the grid was checked for any dependency of the results on the grid. Three semicircular rib cases (that is, coarse, fine, and dense) were modeled to check the grid's independency; these were sufficient to reach grid independency. The fine case, with an interval count of 0.07 (as described in Gambit) and 58,000 quadrilateral cells, was chosen.

## RESULTS AND DISCUSSIONS

Velocity profiles along the  $y$  axes for different  $x$  distances and a high Reynolds number (95,000) is shown in Figure 4. The locations of the profiles are divided to three groups, as shown in Figure 3. The first group crosses the center of the rib in the lower wall and middle distance between the ribs at the upper wall, which at  $x$  equals 40.5, 50.5, 60.5, and 70.5. The second group is located near the surface and downstream of the rib; it is in the lower wall and middle distance between the ribs at the upper wall and at  $x$  equivalent to 42, 52, 62, and 72. However, the third group is placed a middle distance between the ribs at the lower wall and downstream of the rib at  $x$  equals 47, 57, and 67. The  $y$  distance from 0 - 10 is considered the downstream tube while the  $y$  distance from the 14 - 24 is considered the upstream tube. Figures 4a and b show the velocity profiles for profile location just downstream of the rib (42, 52, 62, and 72). The trend of velocity profiles near the lower wall and downstream of

the bend is the same for profiles far from the bend (profiles 42, 52 and 62). The first profile (72) near the bend differs from the others because the velocity maxima are shifted to be nearer the lower wall. This profile also crosses the lowest velocity region. Upstream of the bend, the maximum velocity was shifted to the lower wall as the flow chose the shortest way, creating a high pressure region or stagnation region near the outer wall.

The  $x$  locations 47, 57, and 67 are placed in the front of the upper ribs downstream of the bend and behind the upper ribs upstream of the bend. For the lower ribs, the locations are in the middle, between the ribs. Figures 4c and d show the velocity profiles for these locations (47, 57 and 67). At the first rib downstream and near the upper wall, the velocity is low and increases as it moves in the direction of the flow. Upstream of the bend, the profiles are shaped like the turbulent flow, which is demonstrated to be accurate. The velocity magnitude is higher downstream of the bend because the flow is like a jet after the reduction in area from forming the recirculation at the upper rib.

Figures 4e and f show the  $x$  locations 40.5, 50.5, 60.5 and 70.5, which are in the middle of lower ribs; however, in the upper wall, these profiles are placed midway between the upper ribs. The figures indicate higher velocities near the ribs and drops in velocities as they move toward the upper wall due to the sudden decrease in the duct area. This decrease in the area of flow does not affect the entire width of the duct, but rather only the small area near the rib, as illustrated in the figures. The first profile downstream of the bend differs from others by increasing the velocity near the upper wall due to the formation of recirculation in that position. The flow approaches the end of the bend with a high velocity and momentum, meaning it could not follow the streamlines.

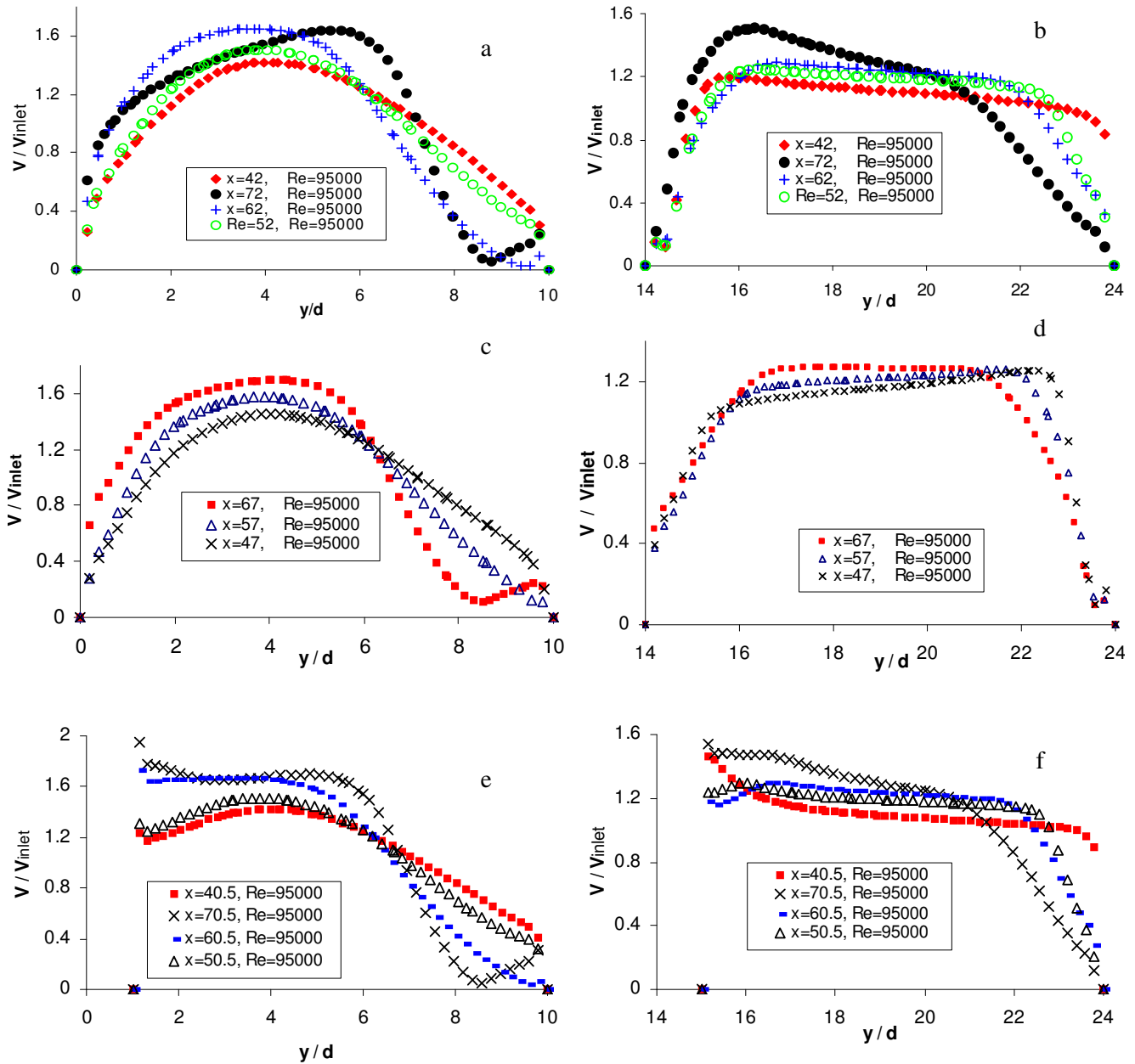


Figure 4. Velocity profile along the  $y$  axes for different  $x$  distances ( $Re = 95,000$ ).

Consequently, this forced the fluid to flow near the lower wall downstream of the bend, creating recirculation in the upper wall and reducing the free stream area of the flow, crooking at the entrance of the downstream duct and near the lower wall beside such recirculation. According to the continuity equation, the velocity will increase in this nick and create different flow and heat phenomena than in the upstream duct, as shown in Figure 5.

The velocity profiles along the  $x$  axes at four  $y$  locations for a high Reynolds number (95,000) are presented in Figure 6. These profiles are located in the middle of the ribs ( $y$  distance). The profile at  $y = 0.5$  crosses the lower

ribs in the downstream duct while the profile at  $y = 9.5$  crosses the upper ribs for the same duct. At the upstream duct, the profile at  $y = 14.5$  crosses the lower ribs and the profile at  $y = 23.5$  crosses the upper ribs. Figure 6a shows the velocity profile at  $y = 0.5$ . The velocity increases gradually after the rib, then makes a sudden decrease just before the rib. Upstream and downstream of the first rib, the velocity is highest in the whole u-tube for the area close to the rib because the fluid does not follow the curvature of the flow but rather travels with most of the flow rate near the lower wall.

At the upper ribs downstream of the bend, the velocity

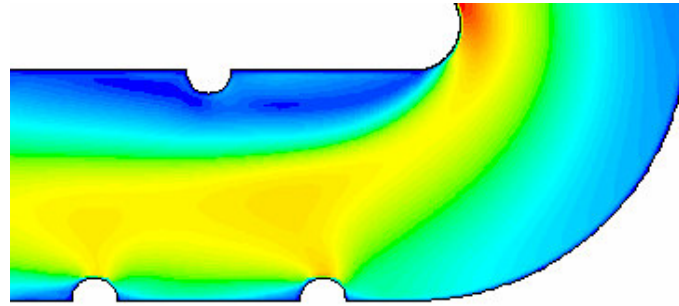


Figure 5. Velocity contours at the entrance of the downstream duct.

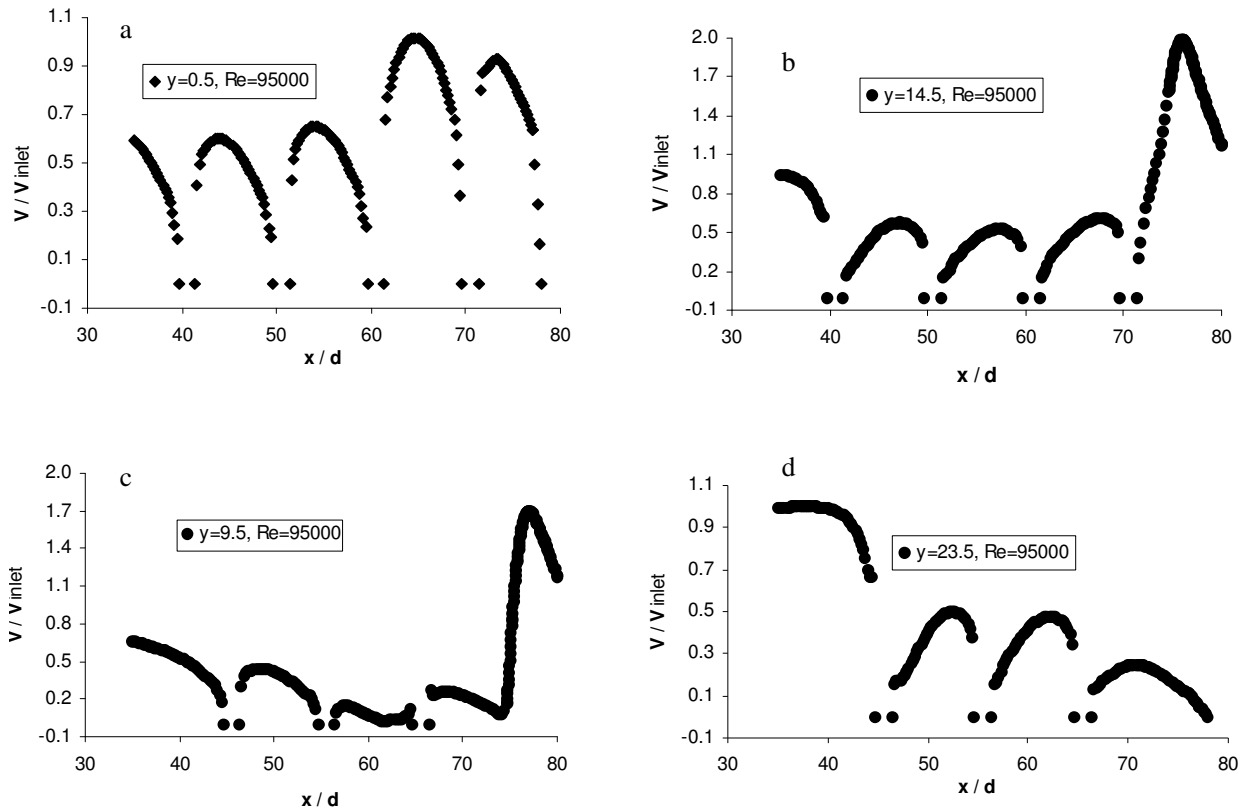
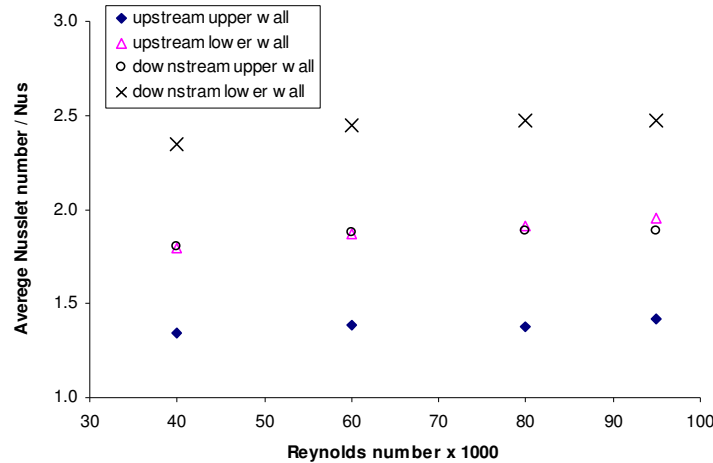


Figure 6. Velocity profile along the x axes at y locations near the four walls (Re = 95000).

magnitudes are the lowest in the entire u-tube, as shown in Figure 6c, due to the centrifugal force acting on the flow when it turns in the bend and then takes a long distance to settle and follow the flow curvature. Furthermore, the lowest velocity occurs just after the first rib. Figure 6b presents the velocity profile at  $y = 14.5$  ( $y_{14.5}$ ) in the upstream duct. The flow here is fully developed and has similar behaviors and velocity magnitudes between each of the two ribs. In addition, behaviors and velocities comparable to  $y_{14.5}$  occur in velocity profile at  $y = 23.5$  and upstream of the bend for the same reasons as shown in Figures 4b and d. The velocity also decreases after the first rib in both walls in the upstream

duct due to the existence of the rib, which increases the width of the boundary layer and creates recirculation between each two ribs.

Figure 7 illustrates the variation in the average of the four Nusselt numbers with the Reynolds number in the u-tube. The highest Nusselt number is close to the lower wall downstream of the bend as the flow moves toward this wall when it is turned in the bend with a high momentum. The upper wall downstream of the bend has the lowest velocity magnitude near the wall; however, the figure shows that this wall has a moderate Nusselt number for two reasons: many recirculations occur at this wall and the average Nusselt number is measured at the wall



**Figure 7.** Variations in the average Nusselt number according to Reynolds numbers for different walls.

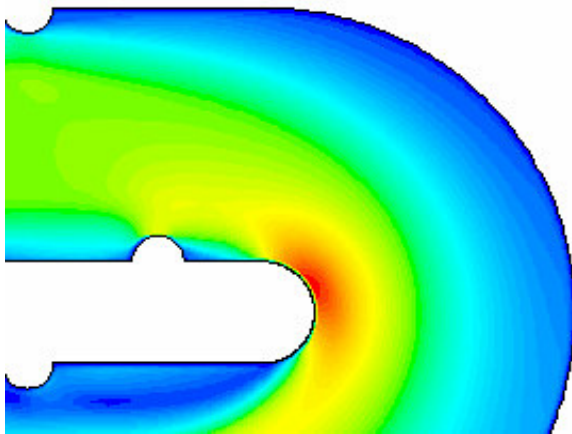


**Figure 8.** The velocity contours the outlet of the upstream duct.

(including the wall at the entrance of the bend) where the velocity is highest before crossing to the lower wall due to the centrifugal force acting during the turn, as shown in Figure 5. The two walls upstream the bend should have the same average Nusselt number because they have similar geometry and flow behavior. However, in the figure, these numbers differ for the same reason as previously explained—namely, the average Nusselt number measured includes the end of the duct and entrance of the bend. Upstream the bend, the velocity increases near the lower wall and decreases close to the upper wall, as shown in Figure 8, because the flow follows the shortest distance. This is evident in the figure when the downstream upper wall has the lowest average Nusselt number. This study measured the whole wall to know exactly where the real heat transfer occurred. It determined that, even if the Nusselt number is divided by the Nusselt number for a smooth pipe, heat transfer was en-

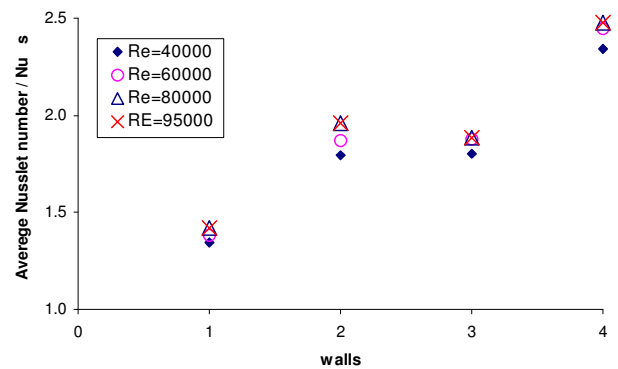


**Figure 9.** Variations in the average Nusselt number according to wall locations at different Reynolds numbers

hanced as the Reynolds number increased.

The ratio of Nusselt number (Nu) for the highest Reynolds number (Re) of 95,000 to Nu for Re of 80,000 is 1.16 while the ratio of Nu for Re 80,000 to Nu for Re 60,000 is 1.3. Furthermore, this ratio is 1.41 for Re 60,000 to the lowest one (40,000). The ratio of the highest Re to the lowest to see the full difference is 1.5. However, the biggest changes in Nu were from Re 40,000 - 60,000. Thus, as the Reynolds number goes higher than a certain value, the increase in Nusselt number increment will be very small. Figure 8 shows the variation of the average Nusselt number according to wall location at different Reynolds numbers. Along the x axes, the number 1 refers to the upper wall in the upstream highest Re to the lowest to see the full difference is 1.5. However, the biggest changes in Nu were from Re 40,000 - 60,000. Thus, as the Reynolds number goes higher than a certain value, the increase in Nusselt number increment will be very small. Figure 9 shows the

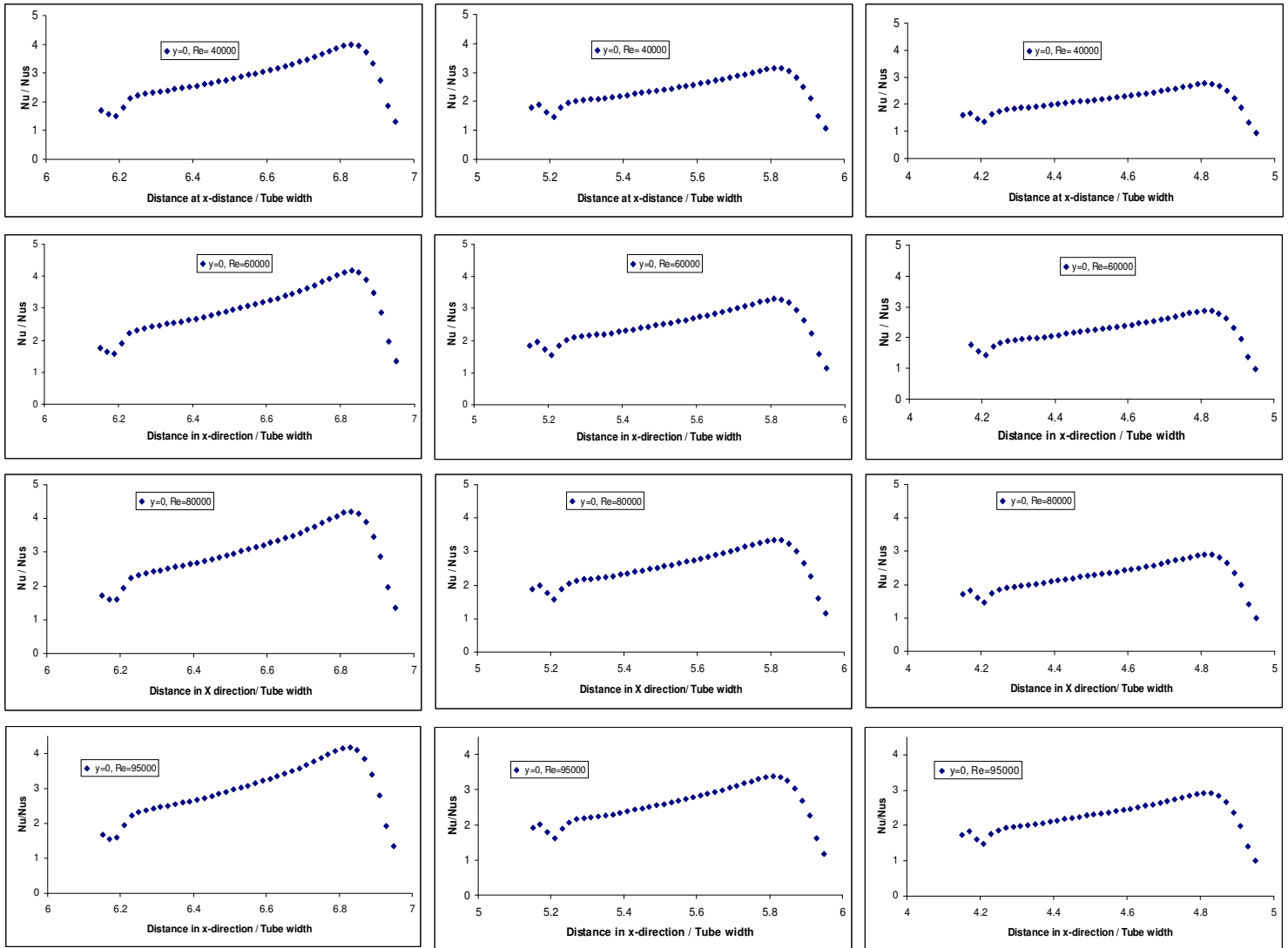


Figure 10. Variation of the Nusselt number between the ribs at  $y = 0$ .

shows the variation of the average Nusselt number according to wall location at different Reynolds numbers. Along the  $x$  axes, the number 1 refers to the upper wall in the upstream duct, 2 is the lower wall in the upstream duct, 3 is the upper wall in the downstream duct, and 4 refers to the lower wall in the downstream duct. Figure 8 shows the wall starting from the middle of the duct to the end of the duct at the bend, covering all the ribs. The Nusselt number is the highest with a maximum Reynolds number. The lower wall downstream has the greatest heat transfer due to reasons previously explained. The lower wall in the upstream duct was second highest due to the high velocity in the bend. In Figures 10 - 13, the  $x$  axes present the location in the wall or the  $x$  distance. The 4 - 5 (lower wall) or 4.5 - 5.5 (upper wall) refer to the distances between the first two ribs. Correspondingly, 5 - 6 or 5.5 - 6.5 refer to the distances between the second and third ribs. Figures 10 and 11 show the variation of the

Nusselt number between the ribs in the downstream duct and at the lower wall ( $y = 0$ ) and upper wall ( $y = 10$ ), respectively. In these figures, the Nusselt number increases just after rib to the peak in the graph (highest  $Nu$ ), then decreases gradually to a position after half of the distance and the flow is reattached due to the recirculations occurring behind the rib when the flow separates at the downstream edge of the rib. The Nusselt number subsequently increases, then decreases just before the next rib as a small recirculation is generated upstream of the next rib. Figures 12 and 13 show the variations in the Nusselt number between the ribs in the upstream duct and at the lower wall ( $y = 14$ ) and upper wall ( $y = 24$ ), respectively. Same heat transfer behaviors in Figures 10 and 11 occur in Figures 12 and 13, which further show that the most enhanced heat transfers occur at  $y = 0$  and between the first two ribs ( $x = 6 - 7$ ). Furthermore, at  $y = 0$ , the highest Nusselt number occurs

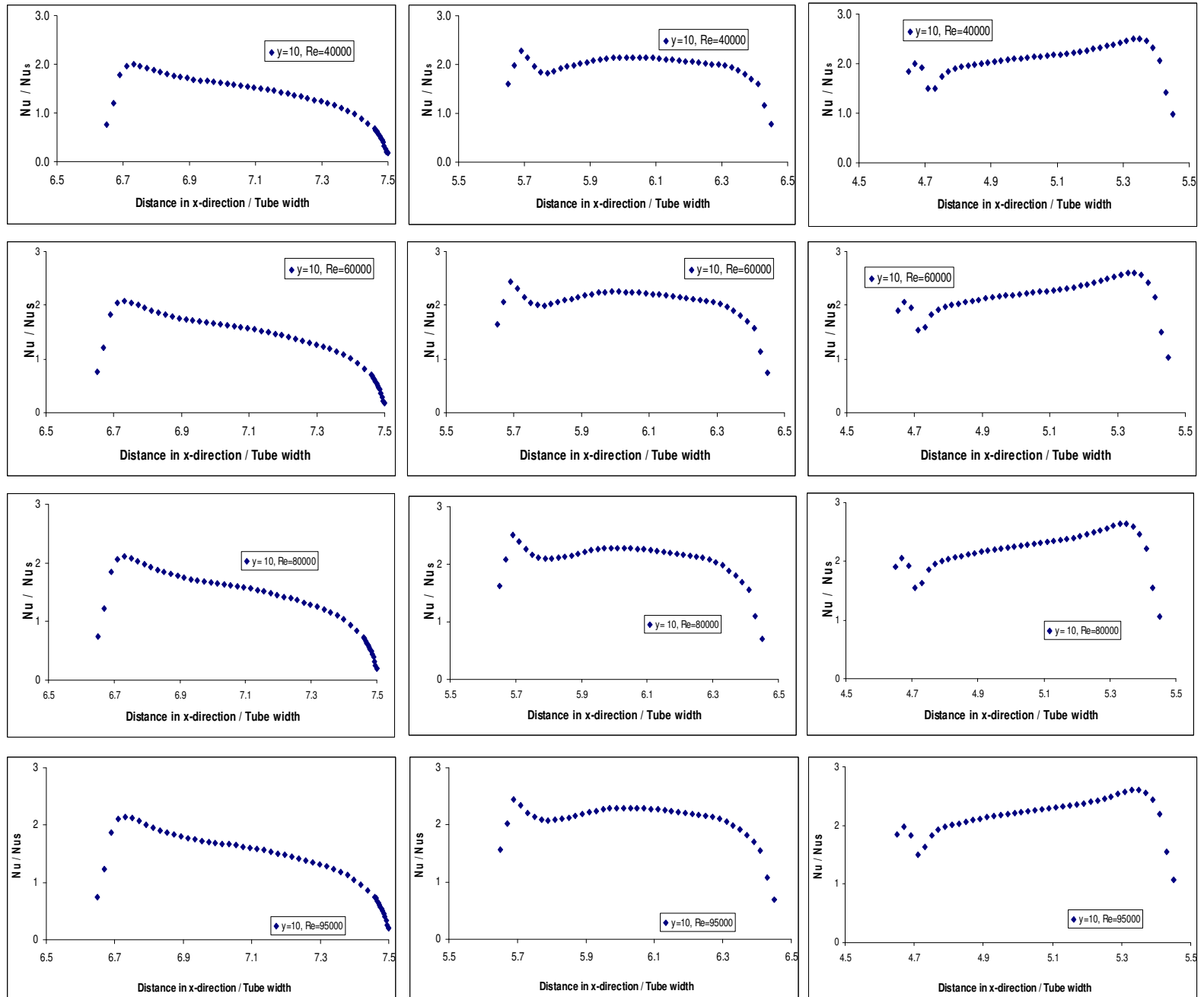


Figure 11. Variation of the Nusselt number between the ribs at  $y = 10$ .

red for the whole  $x$  distance due to fluid flowing in the lower portion of the duct after it turned in the bend, creating a centrifugal force, as previously explained.

**Conclusion**

This study considered the computation of flow and heat transfer in the duct affected by strong curvature and semicircular rib-roughness (turbulators). The turbulators

(ribs) broke the laminar sublayer and created local wall turbulence due to flow separation and reattachment between the ribs, thereby greatly enhancing the cooling effect. The model of the coolant passage consisted of two square ducts connected by a sharp;  $180^\circ$  bend with a rectangular outer wall. Four Reynolds numbers (40,000, 60,000, 80,000 and 95,000) were used in this investigation. In the downstream duct, high velocity regions occurred near the lower wall while very low velocity and large recirculation regions occurred at the upper wall.

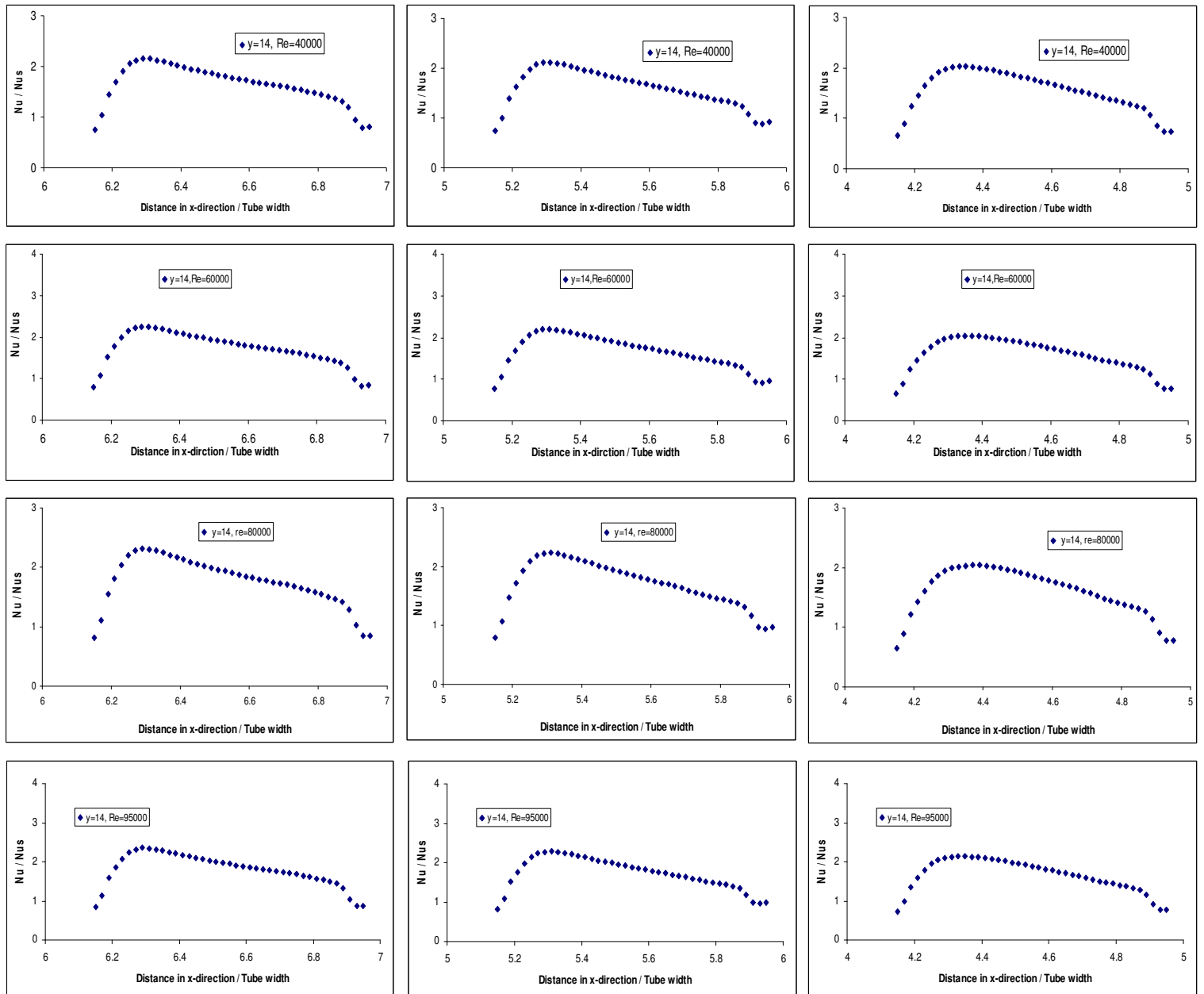


**Figure 12.** Variation of the Nusselt number between the ribs at  $y = 14$ .

However, uniform flow took place in both walls' upstream ducts.

The semicircular ribs improved the heat transfer in the u-tube by increasing the level of the turbulence. The heat transfer was greatest in the downstream duct in both the lower (highest) and upper walls. At the  $x$ -distance, the highest Nusselt number occurred at lower downstream ( $y = 0$ ) due to flow moving with high momentum toward the lower part of the downstream duct creating a centrifugal force. Furthermore, the increment in the Reynolds number enhanced the heat transfer; however, as the Reynolds number increased beyond a certain value (moderate

Reynolds numbers), the increment in Nusselt number was minimized.

#### REFERENCE

- Amro M, Weigand B, Poser R, Schnieder M (2007). An experimental investigation of the heat transfer in a ribbed triangular cooling channel, *Int. J. Thermal Sci.* 46: 491–500.
- Aroon K, Viswanathan AK, Tafti DK (2006). Detached eddy simulation of flow and heat transfer in fully developed rotating internal cooling channel with normal ribs, *Int. J. Heat Fluid Flow* 27: 351–370.
- Besserman DL, Tanrikut S (1992). "Comparison of Heat Transfer Measurements with Computations for Turbulent Flow Around a 180

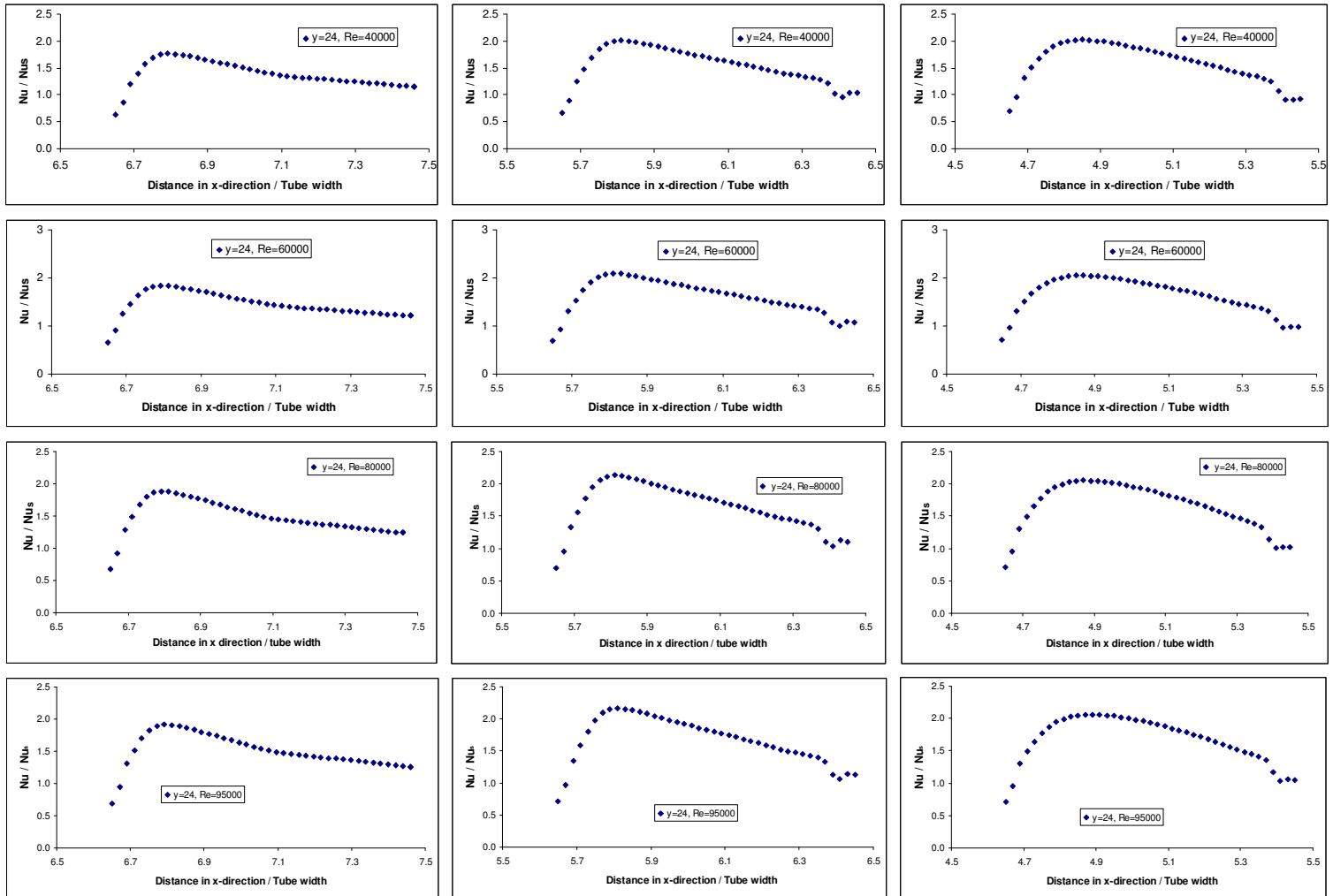


Figure 13. Variation of the Nusselt number between the ribs at  $y = 24$ .

deg Bend," ASME J. Turbomach. 114: 865–871.

Han JC, Dutta S, Ekkad SV (2001). Gas Turbine Heat Transfer and Cooling Technology, Taylor & Francis, London.

Iacovides HB (1995). Launder, Computational fluid dynamics applied to internal gas turbine cooling, Int. J. heat and Fluid Flow, 16: 454-470.

Jia R, Sunden B, Faghri M (2005). Computational Analysis of Heat Transfer Enhancement in Square Ducts with V-Shaped Ribs: Turbine Blade Cooling, J. Heat Transf. 127: 425-433.

Ligrani PM, Oliveira MM, Blaskovich T (2003). Comparison of heat transfer augmentation techniques, AIAA J. 41: 337–362.

Metzger DE, Sahn MK (1986). "Heat Transfer around Sharp 180-deg Turns in Smooth Rectangular Channels," ASME J. Heat Transf. 108: 500–506.

Orszag, S, Yakhot V, Flannery W, Boysan F, Choudhury D, Maruszewski J, Patel B (1993). Renormalization group modeling and turbulence simulations. Proceedings of the International Conference on Near-Wall Turbulent Flows pp.1031- 1042.

Park CW, Lau SC (1998). "Effect of Channel Orientation of Local Heat and Mass Transfer Distributions in a Rotating Two-Pass Square Channel With Smooth Walls," ASME J. Heat Transf. 120: 624–632.

Schabacker J, Bölcs A (1998). "PIV Investigation of the Flow Characteristics in an Internal Coolant Passage With Two Ducts Connected by a Sharp 180° Bend," ASME Paper No. 98-GT-544.

Sewall E, Tafti D (2006). Large Eddy Simulation of Flow and Heat Transfer in the 180-Deg Bend Region of a Stationary Gas Turbine Blade Ribbed Internal Cooling Duct, J. Turbomachinery 128: 763-771.

Tafti DK (2005). Evaluating the role of subgrid stress modeling in a ribbed duct for the internal cooling of turbine blades Int. J. Heat Fluid Flow 26: 92–104.

Taslim ME (2000). Convective cooling in non-rotating and rotating channels – Experimental aspects, VKI-LS 2000-03, Aero-Thermal Performance of Internal Cooling Systems in Turbomachines.

Zhao CY, Tao WQ (1997). "A Three Dimensional Investigation on Turbulent Flow and Heat Transfer Around Sharp 180-Deg Turns in Two-Pass Rib-Roughened Channels," Int. J. Heat Mass Transf. 24: 587–596.